Elastic-Plastic Nonlinear Response of a Space Shuttle External Tank Stringer: Part 1 – Stringer-Feet Imperfections and Assembly

Norman F. Knight, Jr.[1]
General Dynamics Information Technology, Herndon, Virginia

Kyongchan Song[2]
ATK Space Division, Langley Research Center, Hampton, Virginia

and

Kenny B. Elliott[3], Ivatury S. Raju[4], and Jerry E. Warren[5]
NASA Langley Research Center, Hampton, Virginia

Elastic-plastic, large-deflection nonlinear stress analyses are performed for the external hat-shaped stringers (or stiffeners) on the intertank portion of the Space Shuttle's external tank. These stringers are subjected to assembly strains when the stringers are initially installed on an intertank panel. Four different stringer-feet configurations including the baseline flat-feet, the heels-up, the diving-board, and the toes-up configurations are considered. The assembly procedure is analytically simulated for each of these stringer configurations. The location, size, and amplitude of the strain field associated with the stringer assembly are sensitive to the assumed geometry and assembly procedure. The von Mises stress distributions from these simulations indicate that localized plasticity will develop around the first eight fasteners for each stringer-feet configuration examined. However, only the toes-up configuration resulted in high assembly hoop strains.

I. Introduction

THE external tank (ET) of the Space Transportation System (STS) has three main components as indicated in Fig. 1: the liquid oxygen (LOX or LO_2) tank, the intertank (IT), and the liquid hydrogen (LH_2) tank.[1,2] The IT 3 shown in Fig. 2 is a stiffened right circular cylindrical shell structure that connects the LH_2 and LOX tanks and contains the attachment points for the solid rocket boosters (SRBs). The IT is approximately 22.5 feet long and has a diameter of approximately 27.5 feet. The IT shell structure is formed by connecting eight 45° curved panels. Two of these panels are referred to as thrust panels as they house the SRB attachment points, see Fig. 2. The other six panels have external hat-shaped stringers that are fastened to the panel skin, doublers, and chord, see Figs. 3 and 4. These eight panels are assembled together with mechanical fasteners to form the IT structure. The axial position along the ET is given by the coordinate XT in terms of inches. For example, the forward chord flange of the IT is located at XT = 852.8 inches – this location defines the LOX-tank interface.[1,2]

[1] Principal Subject Matter Expert, Structural Mechanics. Fellow AIAA, Fellow ASME.
[2] Structural Analyst, Member AIAA.
[3] Aerospace Engineer, Systems Integration & Test Branch. Member AIAA.
[4] NASA Technical Fellow for Structures, NASA Engineering and Safety Center. Fellow AIAA, Member ASME, Member ASCE.
[5] Aerospace Engineer, Structural Dynamics Branch. Member ASME.

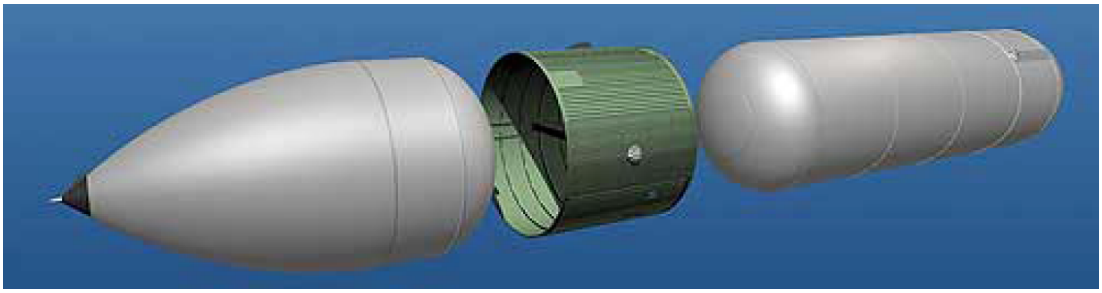

Figure 1. ET basic structural elements (left to right: LOX tank; IT; and LH_2 tank).

During the filling of the ET with cryogenic liquid fuels for the last mission of the Space Shuttle *Discovery*, cracking in the foam on an IT panel near the LOX tank interface was observed.[3] Upon further inspection, it was discovered that not only was the foam cracked, but also two external hat-shaped stringers under that foam on the IT had long cracks along the stringer feet between the fasteners and the stringer sidewall. Detailed three-dimensional (3D) finite element (FE) models are developed and analyzed to investigate the stringer elastic-plastic response and to assess the potential for local failure to develop in the stringer feet.[4]

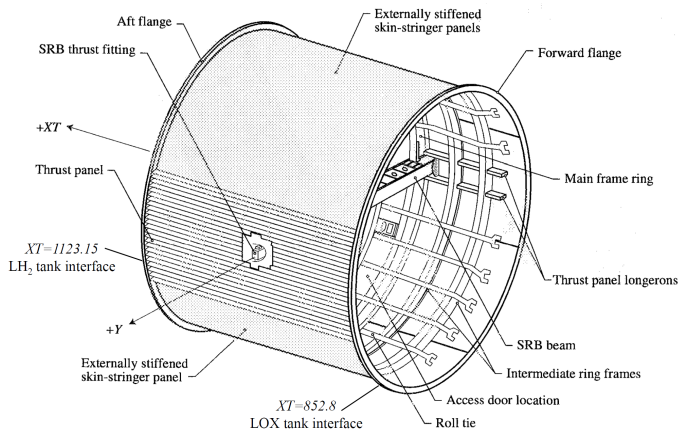

Figure 2. Overview of IT structure (based on Figure 3 in Ref. 2).

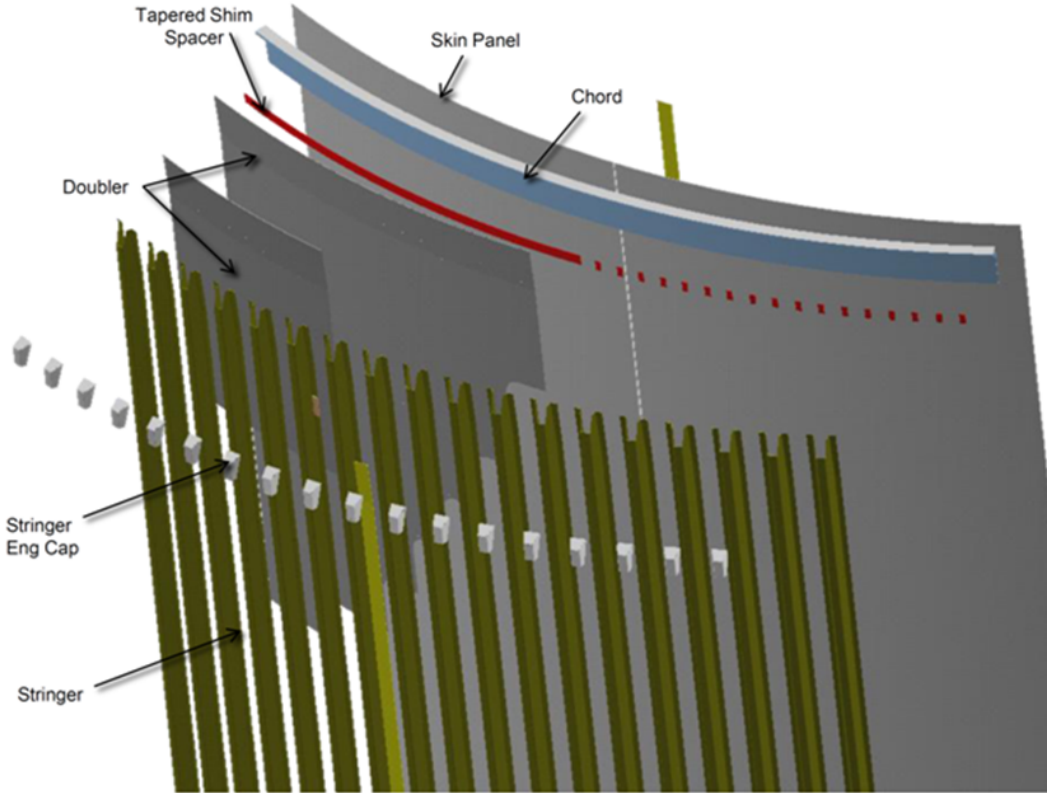

Figure 3. Representative IT panel with external hat-shaped stringers, doublers, spacers, and chord.

Elastic-plastic, large-deflection nonlinear stress analyses are performed for the external hat-shaped stringers (or stiffeners) on the IT portion of the Space Shuttle's ET. These stringers are subjected to assembly strains when the stringers are initially installed on an IT panel. In this paper, an elastic-plastic structural assessment of the assembly process is simulated for an IT stringer at the forward (or LOX tank) end. Specifically, this paper assesses the effect(s) of assembly processes on the elastic-plastic response of the stringer, the influence of stringer-feet imperfections on the assembly strains, and the effect of the radius block installation on the assembly strains. The results of the assembly simulations from this paper are used in conjunction with other operational loads, mechanical and thermal, to assess the IT stringers structural response and to attempt to explain the stringer failure (see Refs. 4 and 5 for details).

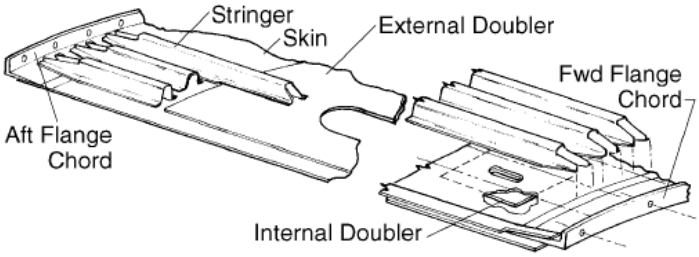

Figure 4. Schematic of a representative IT panel.

II. Structural Analysis Approach

The structural analysis approach followed in the IT stringer failure assessment is the building-block approach illustrated in Fig. 5. A building-block approach is used for developing and anchoring detailed FE analyses. Analyses of the 3-point bend tests (upper left of Fig. 5) performed at the Langley Research Center (LaRC) served as the anchoring point for several modeling and analysis details. The clip tests (upper right of Fig. 5) performed by Lockheed Martin (LM) at the Michoud Assembly Facility (MAF) provided additional correlation data for peak loads and contributed to the formulation of a strain-based failure criterion. Single-stringer models (lower right of Fig. 5) were used to assess various assembly issues including fastener installation sequence, fastener preload, and stringer-feet imperfections. The single-stringer bend test performed at the Marshall Space Flight Center (MSFC) provided test data for model correlation of an assembled stringer and anchored the single-stringer models described in this paper. These single-stringer models were then combined with a partial model of the LOX tank (lower left of Fig. 5), and operational loading cases were evaluated including pre-tanking loading, tanking thermal transient loading, pre-launch loading, and ascent flight loading. Each step in the building-block approach for this application is further described in Ref. 4.

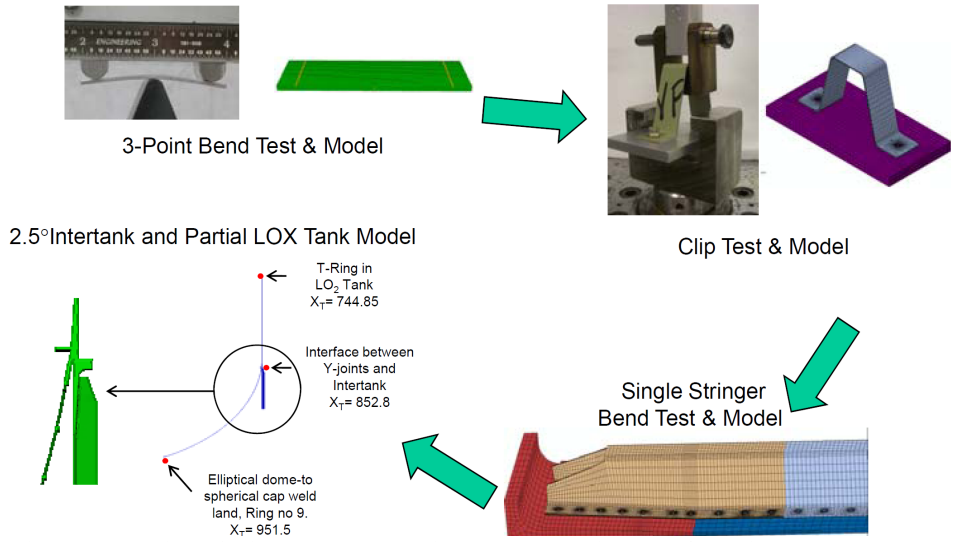

Figure 5. Basic building-block modeling and analysis steps for this assessment.

III. Modeling and Analysis

A. Single-Stringer Modeling

The single-stringer model represents a complete stringer centered within a 2.5° slice of an IT segment at the forward (or LOX tank) end as shown in Fig. 6. Each single-stringer analysis model in the current approach is approximately 45 inches in total length from the mating surface of the forward chord flange (i.e., at XT = 852.8) and extending towards the first intermediate ring frame of the IT (near XT = 897). The single-stringer model, which has 73,514 8-node C3D8I solid elements and 107,908 nodes, is defined as two independent components: a single hat-shaped stringer and a 2.5° slice of the IT LOX-tank end (i.e., IT chord flange, IT skin, and external doublers). In Fig. 6, the tan region represents a typical hat-shaped stringer, and the line within this region on the stringer separates the first ten fasteners nearest the LOX tank end from the aft portion of the stringer model. The forward portion of the stringer model is more refined having four solid elements through the stringer thickness. The green region represents a portion of the IT that includes the forward chord[6], panel skin, and doubler components. These model components are assembled using contact and 36 pairs of fasteners. Specific IT skin thickness values and doubler configuration details (i.e., no doublers, a single doubler, or double doublers) depend on the circumferential location of the 2.5° segment around the IT. The two component models are assembled using mostly rivets away from the stringer ends. Near the stringer ends, a combination of GP® [7] lock bolts and Hi-lok® [8] fasteners are installed. A cylindrical coordinate system is created and used to assign boundary conditions. Symmetry boundary conditions are imposed on both circumferential faces of the IT model and along the axial end away from the IT chord flange. The mating surface of the IT chord flange is free.

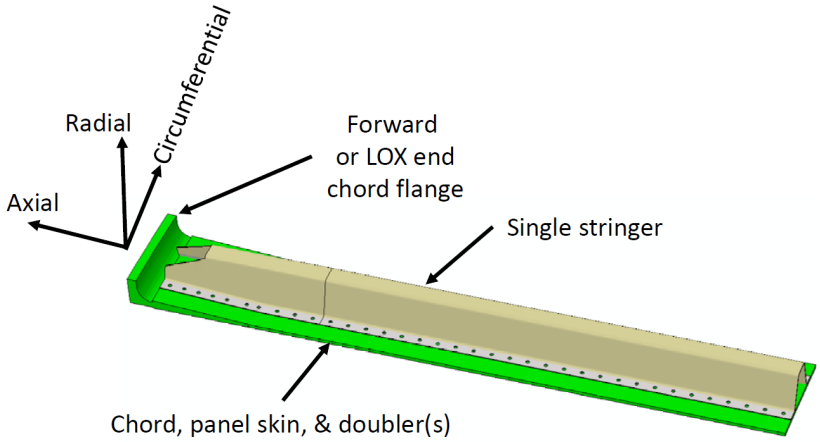

Figure 6. Representative 3D model of a single-stringer configuration: single stringer with portion of the IT (2.5° slice).

The FE mesh for the IT region up to the first ten fasteners has several 8-node C3D8I solid elements through the thickness, and then as the chord runs out, there are only two elements through the thickness of the skin/doubler combination. This transition occurs beyond the region of interest, and results consistent with uniform refinement were confirmed. The hat-shaped IT stringer, denoted by the tan region in Fig. 6, is also independently modeled as a separate structural component. The entire stringer length was initially modeled with four 8-node C3D8I solid elements through the stringer thickness. However, to reduce the computational size of the problem, only a single element through the stringer thickness was used beyond the tenth fastener based on results from mesh convergence studies. The dissimilar FE meshes through the thickness were combined using tied kinematic constraints within ABAQUS™/Standard[9].[6] These independent FE models are assembled, and surface-to-surface 'hard' contact is assumed between the skin/doubler outer surface and the bottom surface of the stringer feet. Small sliding is permitted, and an aluminum-to-aluminum dry static coefficient of friction is used. The current single-stringer FE model has roughly 1.3 million degrees of freedom (DOF).

B. Material Modeling

For elastic-plastic structural response, the elastic mechanical properties are, in general, augmented by providing uniaxial tensile stress-strain data obtained from coupon-level mechanical testing. The IT material properties for aluminum lithium 2090-T83 were obtained from MSFC for room temperature and -25°F.[7] The elastic material properties are listed in Table 1, and the nominal uniaxial stress-strain curves for room temperature and -25°F are

[6] The forward chord provides a flange for mating with the LOX tank. The length of the forward chord depends on the circumferential IT location: in some cases, it is a 'long' chord approximately 7 inches long, while in other locations it is a 'short' chord approximately 5 inches long.
[7] GP is a registered trademark of Huck International, Inc., Tucson, AZ.
[8] Hi-lok is a registered trademark of Hi-Shear Corporation, Torrance, CA.
[9] ABAQUS™/Standard is a registered trademark of Dassault Systèmes Simulia Corp.

shown in Fig. 7. Data for the T-orientation are used in these analyses. Table 2 lists the Al 2024-T81 material properties[8] used for the radius blocks. The analyses include the elastic-plastic, temperature-dependent stress-strain data for the IT components. The input to ABAQUS™ is the true stress as a function of plastic strain in a piecewise linear approximation for each specified temperature. Because the response is a single loading event with some, but not complete, load reversal expected, the response is a single cycle and isotropic strain hardening is assumed, and the influence of the Bauschinger effect is neglected. In addition, the material could be approximated as elastic, perfectly plastic in which case isotropic and kinematic strain hardening rules predict identical results.

In a multi-axial stress state, when the effective stress exceeds the initial uniaxial yield stress, yielding is assumed to occur, and the subsequent local strain state will include elastic and plastic contributions. The incipient yielding is determined using von Mises or Tresca's criterion. As the loading is further continued past the yield point, subsequent yielding progresses – yield surface expands (strain-hardening materials) or the yield surface translates (kinematic hardening) or the yield surface remains constant (elastic-perfectly plastic materials). For isotropic strain hardening, the yield surface expands as the plastic strain increases. Within a 3D stress analysis, the effective stress is calculated and the yield criterion evaluated. Once initial yielding is detected using the effective stress, the individual strain components will exhibit a plastic or residual, or non-recoverable part even though the individual total mechanical strain components may be small enough to *appear* to be elastic because dislocations along other planes have occurred.

Table 1. Material properties for the IT stringers – nominal Al-Li 2090 T83.[7]

	Room Temperature	-25°F
Elastic modulus, Msi	11.5	11.8
Poisson's ratio	0.3	0.3
Coefficient of thermal expansion, in./in./°F	12.2×10^{-6}	11.7×10^{-6}

Table 2. Material properties for the radius blocks – Al 2024-T81.[8]

	Room Temperature	-320°F
Elastic modulus, Msi	10.5	11.76
Poisson's ratio	0.33	0.33
Coefficient of thermal expansion, in./in./°F	12.2×10^{-6}	9.8×10^{-6}

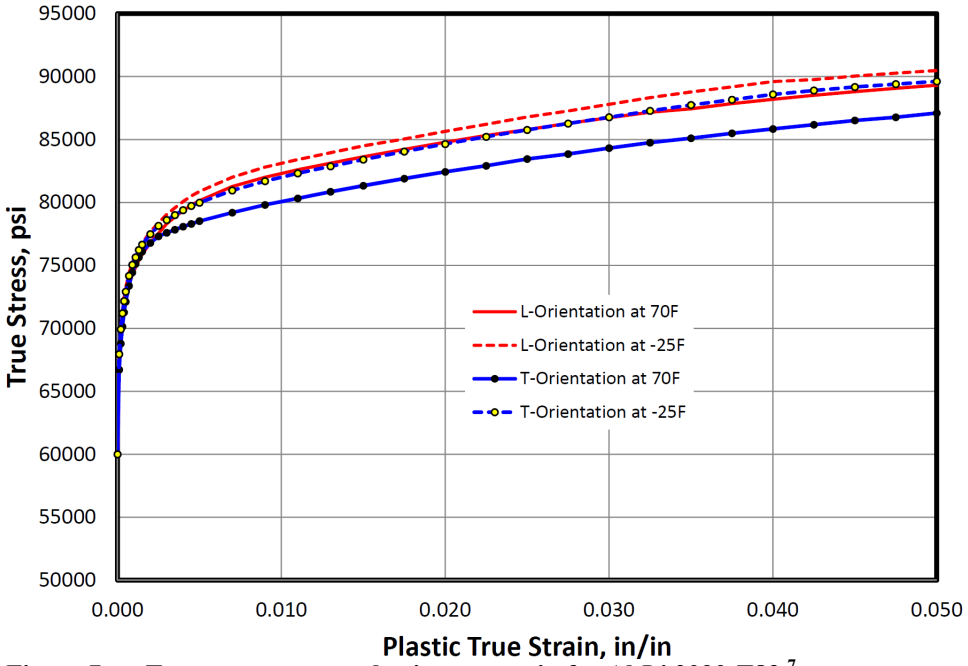

Figure 7. True stress versus plastic true strain for Al-Li 2090-T83.[7]

C. Fastener Modeling

The FE models of these two components (i.e., chord/skin/doubler and stringer) are 'connected' through a fastener installation assembly for 36 pairs of fasteners along the stringer feet – 72 fasteners in total for the current FE model of a single stringer. Counting from the aft end of the model towards the forward flange, there are 28 pairs of rivets, three pairs of Hi-lok® fasteners, and then five pairs of GP® lock bolts. In the fastener installation simulation, pairs of fasteners are 'installed' simultaneously – one on each stringer foot at the same axial location. All rivets are installed first, followed by pairs of Hi-lok® fasteners, and then pairs of GP® lock bolts.

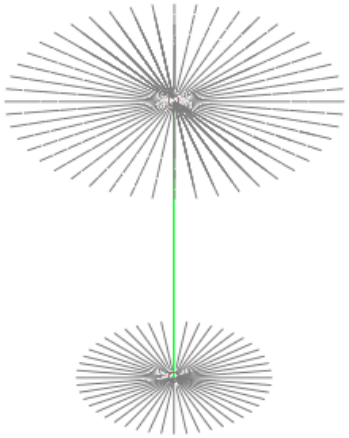

Figure 8. Typical fastener modeling using beam elements and kinematic-coupling constraints referred to as beam-spider modeling.

Each fastener is modeled as a set of linear elastic beam elements for the fastener shank and kinematic-coupling constraint sets for the fastener head and the end cap or nut as indicated in Fig. 8. Each constraint set defines a set of nodes, typically within a single plane, that translate according to the reference node and are free to rotate as a plane with the deformable top surface of the stringer feet. Kinematic coupling automatically constrains the nodal DOF on a surface to a reference node. In these models, nodes of one bounding surface corresponding to the chord/skin/doublers are tied to the reference node at one end of the beam element modeling the fastener. Those nodes on the top surface of the stringer feet are tied to the reference node at the other end of the beam modeling the fastener. Nodes through the thickness and along the hole boundary are not constrained, and contact between the fastener hole boundary and the fastener shank is not modeled. The fastener holes are not explicitly represented in the FE model of the chord/skin/doubler component; the beam element representing the fastener shank penetrates this region and a set of kinematic-coupling constraints are defined on the bounding surface. The kinematic-coupling constraints thereby define a rigid plane that permits translation and rotation. In the current models, the kinematic-coupling constraints imposed on the top surface of the stringer feet involve nodes within a 0.389-inch-diameter region of the fastener hole centerline, and those on the skin/doubler region involve the nodes connected to the reference node of the beam (i.e., 8 nodes on four adjacent solid element faces). This fastener modeling approach is further described in Refs. 9 and 10, and general FE modeling of fasteners is discussed in Ref. 11.

D. Stringer-Feet Imperfection Modeling

The fabrication of the IT external hat-shaped stringers is a multi-step process that starts with a sheet that is cold rolled to a general hat shape and then hot formed to the specific dimensions and final shape. An added installation complication is that the stringer is fabricated with an upward bend on both ends to accommodate tapered IT chord flanges on the LOX and LH_2 ends of the IT. This bend occurs roughly at Fastener 7 for regions with a long chord. From Fastener 7 to the front end, different stringer-feet imperfections may occur with the peak imperfection possibly occurring at the stringer ends and tapered linearly down to the flat-feet configuration at Fastener 7 (i.e., the imperfection is uniformly tapered over the flange chord length). The implication of this assumption is that stringer-feet imperfections have little or no influence on the response of Fastener 8 and beyond.

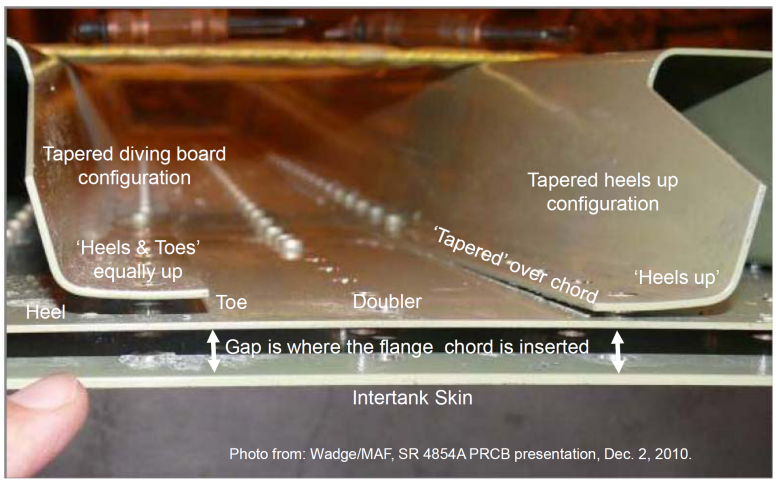

Figure 9. Various stringer-feet imperfections. Photograph courtesy of Mr. G. Wadge/LM-ET.

A stringer foot has a heel (i.e., transition between foot and region close to the stringer sidewall) and a toe (i.e., region close to the stringer free edge) as shown in Fig. 9. The center of the fastener holes is 0.44 inches from the

stringer free edge. The baseline configuration is assumed to be a stringer with flat feet. In this configuration, the stringer feet would sit perfectly on a flat surface; however, because the stringers are installed on the curved IT surface, which has a large radius, the stringer feet are not in full contact with the IT surface. The flat-feet configuration for the IT installation can result in an inherent toes-up condition simply due to the stringer feet being flat and then installed on a cylindrical surface (i.e., in these FE models, toes are initially up approximately 18 mils, and the heels are up approximately 9 mils from the curved IT surface for the baseline flat-feet configuration).

Four stringer-feet imperfection configurations are shown in Fig. 10. The baseline flat-feet configuration shown in Fig. 10a exhibits a toes-up condition due to the IT curvature. The heels-up configuration shown in Fig. 10b is defined as the configuration when the heels of the stringer feet at the end of the stringer are offset either 20, 40, or 60 mils further from the flat-feet configuration, while the stringer toes remain in the flat-feet configuration and linearly tapered across the stringer foot. The diving-board configuration shown in Fig. 10c has the heels and toes offset either 20, 40, or 70 mils from the flat-feet configuration (i.e., uniform offset with no tapering across the stringer foot). The toes-up configuration shown in Fig. 10d is when the toes of the stringer feet at the end of the stringer are offset either 20, 40, or 60 mils further away from the flat-feet configuration, while the stringer heels remain in the flat-feet configuration (linearly tapered across the stringer foot). However, the toes-up configuration has not been observed based on the inspection of spare stringers inventoried at MAF.[10] While the toes-up condition may be possible, it would represent an unusual fabrication and/or installation end product.

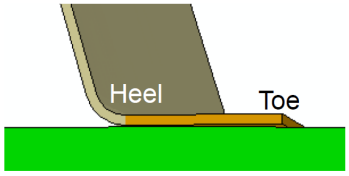

Heels not in contact with surface; installation tool pushes stringer heels to surface; fasteners then installed

a) Baseline flat-feet configuration.

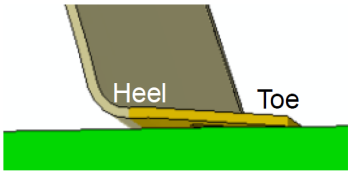

Heels not in contact with surface; installation tool pushes stringer heels to surface; fasteners then installed

b) Heels-up configuration.

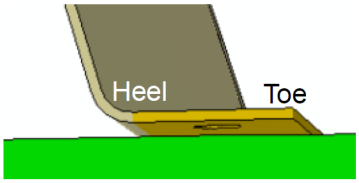

Heels not in contact with surface; installation tool pushes stringer heels to surface; fasteners then installed

c) Diving-board configuration.

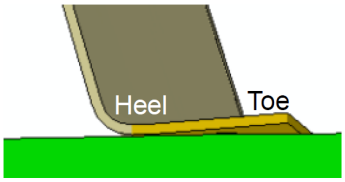

Heels already nearly in contact with surface; installation tool has minimal effect; fasteners need to pull toes down

d) Toes-up configuration.

Figure 10. Baseline and three stringer-feet imperfection configurations.

The stringer configurations analyzed assume the same imperfection for both stringer feet. Imposing different stringer-feet imperfection types and/or imperfection amplitudes for the left and right stringer feet poses no additional analytical difficulty. However, a systematic approach to assess such a non-deterministic problem was not developed due to the lack of stringer-feet imperfection data.

E. Fastener Installation Simulation

The IT assembly process consists of the following steps. First, the stringer end is aligned at the LH_2 flange end. Then, rivets are installed from the center portion of the IT panel towards the ends. Next, the stringer hat near the stringer end is pushed down to the panel surface with a clamp screw assembly fixture shown in Fig. 11, and a drill jig is used to drill holes. The push-down displacement is dependent on the

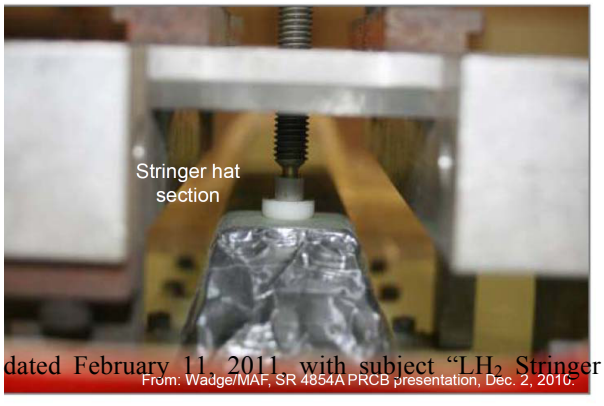

Figure 11. Stringer installation tool to push the stringer feet to IT surface.

[10] Based on email from Steven G. Holmes, MSFC, dated February 11, 2011, with subject "LH_2 Stringer End Flatness".

local stringer-feet configuration. Then, it is assumed that the Hi-lok® fasteners are installed after the rivets, followed by the installation of the four pairs of GP® lock bolts. During the preloading of the last pair of GP® lock bolts (i.e., Fastener 1), the stringer hat push-down displacement is removed.

This fastener installation simulation attempts to mimic the assembly process just described. The single-stringer FE model is positioned over the IT panel FE model. After positioning the stringer, all rivets are installed (28 pairs of rivets for this FE model) and preloaded to 200 pounds in the simulation. This rivet preload value alleviated some of the numerical convergence issues that arose during the nonlinear iterations for the initial contact determination of these two independent FE models. Values of preload greater than 200 pounds for the rivets produced nearly the same results. After the rivet installation is simulated, the push-down process is simulated by imposing a transverse applied displacement to a small central region on the stringer hat section outer surface approximately 0.5 inches from the end as indicated in Fig. 12. This rectangular region is defined by 18 surface nodes of ten adjacent solid element faces as indicated in Fig. 12 and covers an area of approximately 0.15 in^2. The magnitude of the applied push-down displacement in these simulations is at least 5 mils even for the flat-feet configuration. However, the value is dependent on the stringer-feet imperfection configuration.

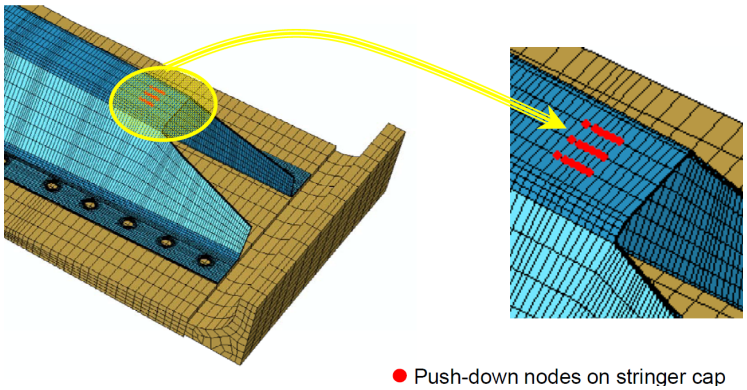

Figure 12. Location of the FE model push-down nodes.

Once the stringer is pushed down, three pairs of Hi-lok® fasteners are installed and preloaded to 2350 pounds. Subsequently, four pairs of GP® lock bolts are installed and preloaded to 3300 pounds. The last pair of GP® lock bolts are installed simultaneously as the applied push-down displacement is released. At the end of this solution step, only the fasteners and the rivets are holding the stringer to the IT segment.

F. Radius Block Installation

During the IT repair process following the cracking of the stringer feet on ET-137 prior to the STS-133 mission, radius blocks (see Fig. 13) are installed on most of these stringers on the IT/LOX-tank end. The simulation of the radius block installation reported here is for a 6-hole radius block[11] covering six fastener locations (i.e., Fasteners 2 through 7).[12] After the basic fastener installation simulation is completed, Fasteners 2 through 7 on each stringer foot are unloaded (i.e., their preload is removed) in one ABAQUS™ solution step, and then the radius blocks for each stringer foot are positioned and installed using 0.25-inch-diameter blind A286 steel fasteners with a preload of 290 pounds in a second solution step. These two additional solution steps complete the fastener installation and assembly process simulation for cases when radius blocks are installed.

[11] In locations with a short flange chord, shorter 4-hole radius blocks are installed.

[12] Also note that Fastener 1 is untouched while Fasteners 2 through 7 are removed and the radius blocks are installed.

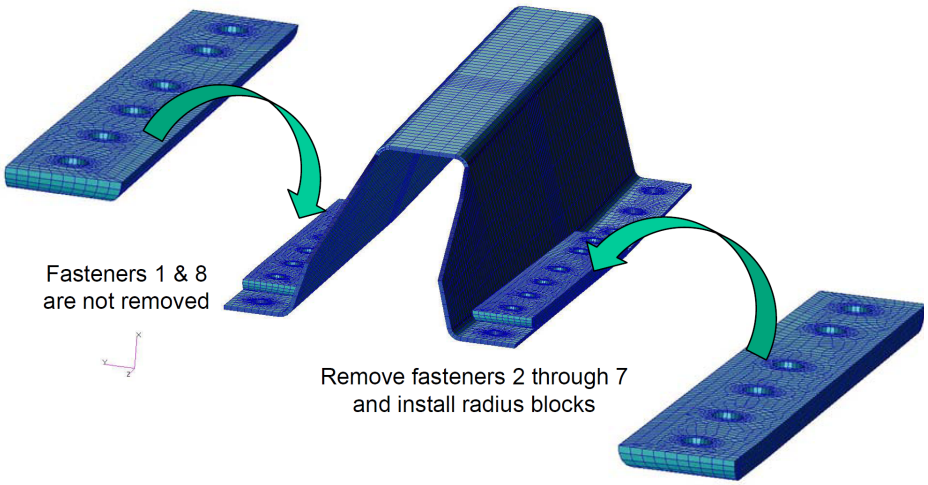

Figure 13. Radius blocks for the IT LOX end long chord configuration.

IV. Numerical Results and Discussion

Elastic-plastic, nonlinear stress analyses are performed using ABAQUS™, and the results are discussed in this section. Assembly or fit-up stress and strain response of a single stringer has been simulated for the baseline flat-feet configuration as well as for three different types of stringer-feet imperfections with different imperfection amplitudes. To characterize the influence of the stringer-feet imperfection, peak values of strain in a subset of elements on the bottom of the stringer foot near the first eight fasteners are compared. These subsets of elements are beyond the fastener head and are shown in red in Fig. 14. Note that these elements are not included in the kinematic coupling constraints for the fastener modeling.

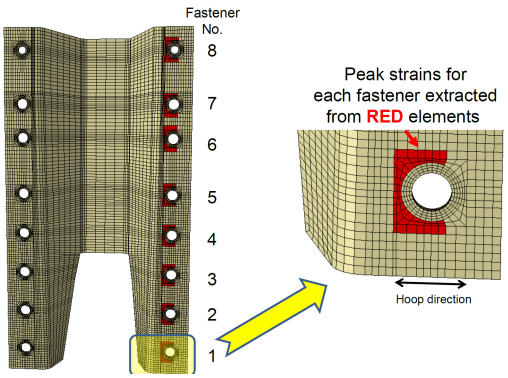

Figure 14. Selected element subgroups for strain recovery during the assembly simulation – red elements denote the fastener element group used to extract peak strain values near each fastener.

The strain components extracted from the computational database at each of the eight element integration points within a solid element are compared, and the peak total strain value is identified within each fastener group of elements (i.e., each subgroup of red elements highlighted in Fig. 14). The strains reported for the fastener assembly simulation are the total strains. Note that the total strain is the sum of the elastic and inelastic components. For these analyses, the strain due to creep is neglected, and the inelastic strain represents only the plastic strain. Two types of strain components are examined: total hoop strain and maximum principal total strain. The total hoop strain component is across the stringer feet in the circumferential or hoop direction of the IT shell (see Fig. 14). Positive hoop strain values on the bottom of the stringer feet would tend to 'open' a defect if and when it forms and if the defect is aligned normal to the hoop direction. By selecting elements adjacent to but not under the fastener head (i.e., the red elements indicated on the right side of Fig. 14), elements having peak through-the-thickness (or transverse normal) strains caused by preloading the fasteners are excluded from the direct comparison. However, all elements are automatically included in the contour plots to be shown. Large through-the-thickness normal stresses resulting from the fastener installation and preload conditions contribute to the effective or von Mises stress that is used to determine analytically the onset of local yielding.

A. Assumptions for the Single-Stringer Simulations

The following assumptions are made in these assembly simulations:

- Linear taper of the stringer-feet imperfection while the stringer is over the forward long chord (over the first seven fasteners) with no imperfection beyond Fastener 8;
- Three types of stringer-feet imperfections (i.e., heels up, diving board, and toes up);
- An applied displacement on the stringer hat to push the stringer to the IT panel surface;

- Applied displacement magnitude defined by the distance the heels were initially displaced from the IT panel surface;
- Fastener installation in pairs from Fastener 8 location to Fastener 1 location;
- Maximum fastener preload values applied;
- Fastener head diameter of 0.389 inches; and
- Stringer thickness of 0.056 inches.
- IT panel skin thickness of 0.083 inches.
- Total double doubler thickness of 0.146 inches.

All of the stringer-feet imperfection configurations shown in Fig. 10 have a linear 'tapered' distribution from the maximum imperfection amplitude at the stringer end near Fastener 1 to the baseline flat-feet configuration between Fasteners 7 and 8. As discussed previously, the stringer hat, in all cases, is 'pushed' down towards the IT panel at least 5 mils after the rivets are installed and preloaded. Only the toes-up configuration (see Fig. 10d) after the 'push down' has a significant initial gap to close at the stringer-feet toes because the stringer-feet heels are already nearly in contact prior to any push-down loading.

Assembly analyses are performed for the LOX end stringers with the IT long chord, nominal fastener installation, and other nominal configurational details. Note that there are several possible configurations with an IT short chord, off-nominal fastener installation, and other off-nominal configurational details such as, different panel thicknesses, stringers from the LH_2 tank end of the IT, non-alignment of the stringers on the LOX tank end, etc. Many of these off-nominal configurations could result in higher assembly strains. Assembly analyses of these myriad off-nominal configurations were not attempted.

B. Influence of Stringer-Feet Imperfection Type

The influence of the stringer-feet imperfection type on the stringer end's deflected shape after assembly is examined for the four different stringer configurations shown in Fig. 10. Note that the end of the stringer has a tapered sidewall height without a hat section until just beyond Fastener 3 (see Fig. 15). Therefore, the stringer sidewall sections are free and unsupported for the first three fasteners near the end of the stringer.

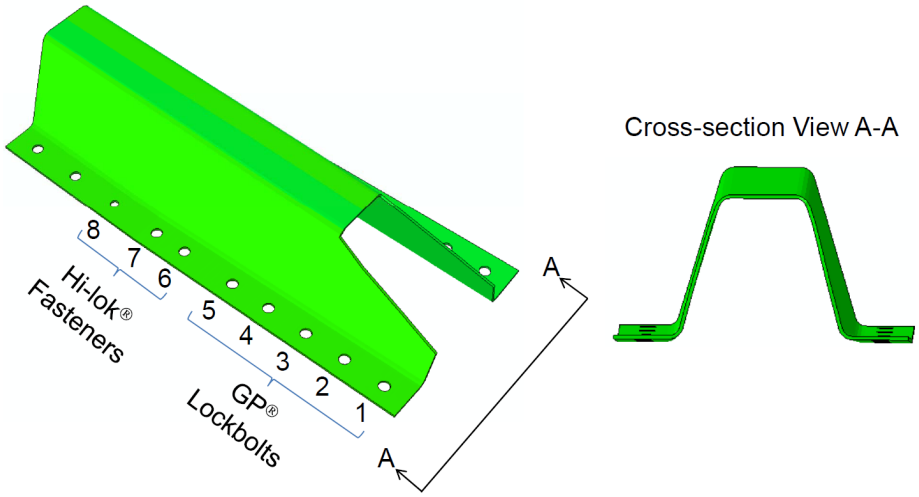

Figure 15. Baseline flat-feet stringer configuration with a cross-sectional view.

Scaled deformed shapes of the stringer end cross-section are shown in Fig. 16 for the four different stringer-feet configurations. The nodal displacements of the stringer measured from their original nodal locations are scaled by a factor of five in order to visualize the different deformed shapes resulting from assembly. Contour plots of the 'near' circumferential or hoop displacement component U2 are shown on the deformed shape as well with peak values being ±0.056 inches – the stringer thickness – indicating a large-deflection nonlinear analysis is required.[13] The response of the baseline, flat-feet configuration due to assembly is shown in Fig. 16a. The feet toes deflect towards the IT surface and the stringer sidewalls deflect slight outward. The response of the heels-up 60-mil configuration

[13] A nonlinear analysis is required due to the inclusion of surface-to-surface contact and elastic-plastic material response even if the deflections are small (i.e., less than half the panel thickness). However, some analysis tools provide an option to use either a small- or large-deflection formulation in the simulations, and in the analyses performed for these studies, the large-deflection capability is required and selected.

due to assembly is shown in Fig. 16b. The feet heels deflect towards the IT surface as a result of the 'push down' and the stringer sidewalls deflect inward with a peak deflection of roughly half the stringer thickness indicating the onset of large deflections. The response of the diving-board 70-mil configuration due to assembly is shown in Fig. 16c indicating a more uniform deflected shape for the stringer feet and a slight outward bending of the stringer sidewalls – more than for the flat-feet configuration but still small deflections. Finally, the response of the toes-up 60-mil configuration due to assembly is shown in Fig. 16d. The feet toes deflect towards the IT surface and the stringer sidewalls deflect significantly outward with a peak deflection more than the stringer thickness thereby requiring a large-deflection nonlinear analysis.

Fractography results[12] indicated that crack initiation likely occurred on the bottom of the stringer feet. Therefore, the analytical studies examined the elastic-plastic response on these surfaces. A comparison of the von Mises stress distributions on the bottom surface of the stringer feet for the flat-feet configuration and the different stringer-feet imperfection configurations with the maximum imperfection amplitude is shown in Fig. 17 for the first eight fasteners from the stringer end. In these contour plots, the contour levels range from zero as blue to values greater than 60,000 psi as red denoting the uniaxial stress level for the initial onset of yielding. These contour plots indicate that the uniaxial initial yield stress has been reached or exceeded in the vicinity of the fastener holes for all stringer-feet configurations. Only the toes-up configuration shown on the right side of Fig. 17 exhibits large high-stress regions around the GP® lock bolts (i.e., first five fasteners) that extends beyond the fastener head. These results indicate that localized plasticity will develop, as a minimum, around the first eight fasteners.

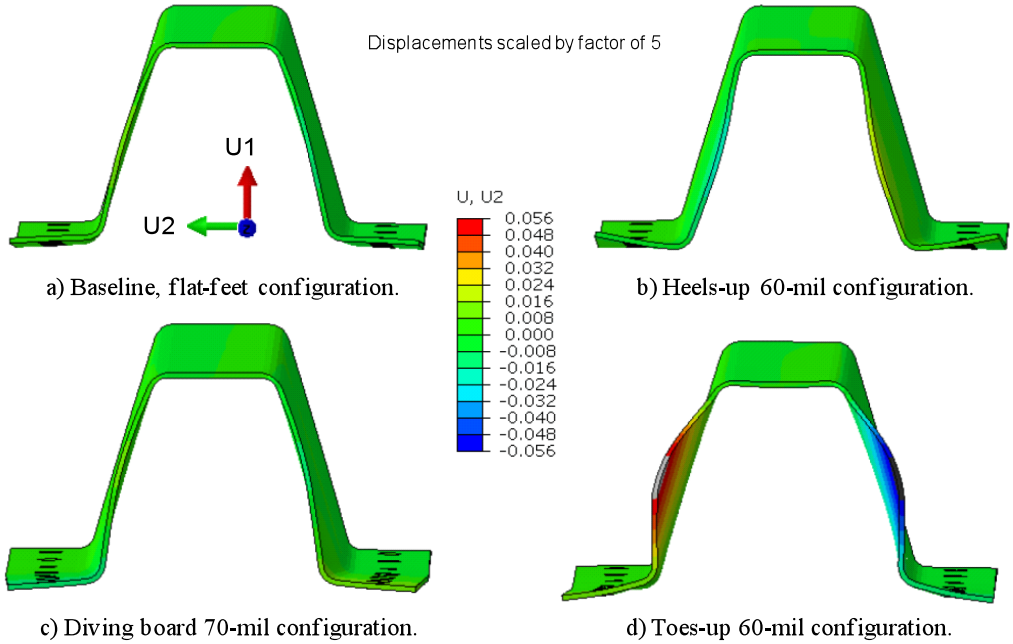

a) Baseline, flat-feet configuration.

b) Heels-up 60-mil configuration.

c) Diving board 70-mil configuration.

d) Toes-up 60-mil configuration.

Figure 16. Cross-sectional views of the deformed shape of the forward end of the stringer after the assembly simulation.

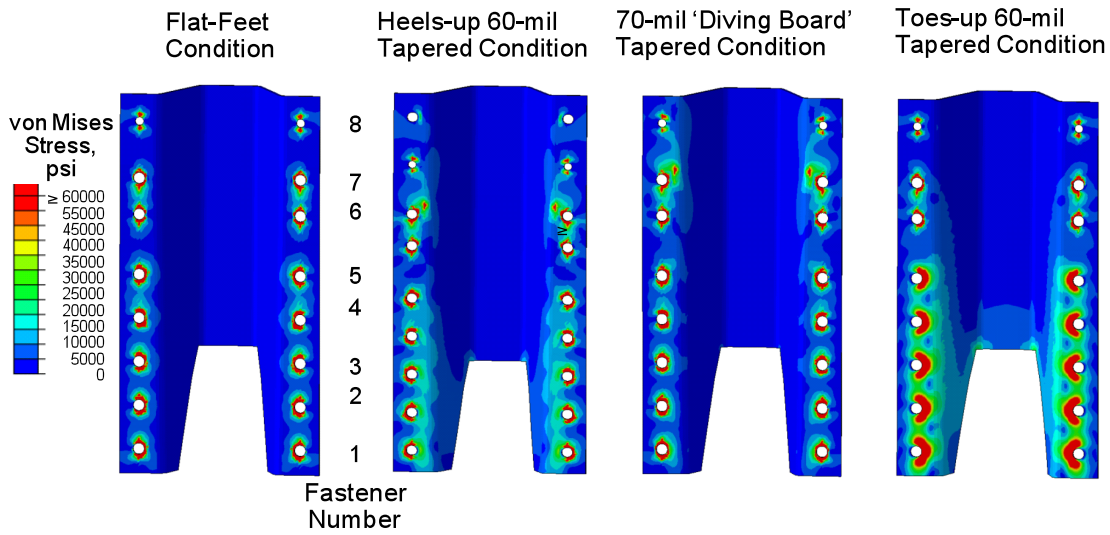

Figure 17. Von Mises stress distributions for the first eight fasteners after assembly – stringer-feet bottom surface.

A comparison of the total hoop strain distributions on the bottom surface of the stringer feet for the flat-feet configuration and the different stringer-feet imperfection configurations with the maximum imperfection amplitude is shown in Fig. 18 for the first eight fasteners. In these contour plots, the contour levels range from values more negative than -0.005 in./in. (compression) shown as blue to values greater than 0.005 in./in. (tension) shown as red. The uniaxial strain at the elastic limit for this material is 0.005 in./in. or 0.5 percent. These results clearly indicate that only the toes-up configuration results in total hoop strains exceeding the uniaxial elastic strain limit and causing local yielding due to hoop strain alone. However, the results shown in Figs. 17 and 18 indicate that a combined stress state exists, and an elastic-plastic response near the first eight fasteners is anticipated to occur during the assembly step. Material testing has indicated that Al-Li 2090-T83 from suspect heat-treatment lots had a higher initial yield stress and a brittle fracture behavior just after initial yielding.[13,14] Hence, these analysis results indicate the potential for an assembly strain level higher than the elastic limit.

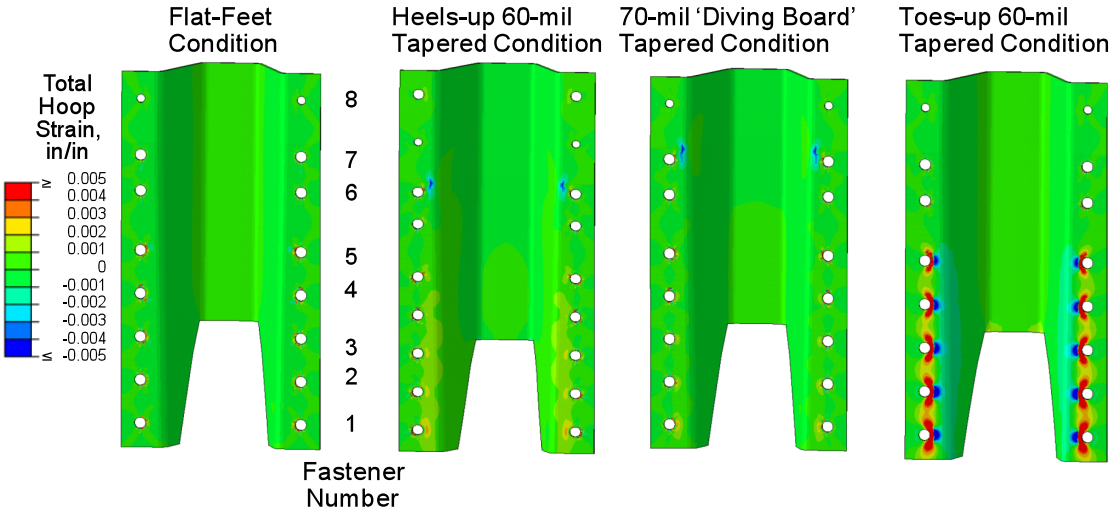

Figure 18. Total hoop strain distributions for the first eight fasteners after assembly – stringer-feet bottom surface.

C. Effect of Stringer-feet Imperfection Amplitude

The previous results are for the maximum stringer-feet imperfection amplitude for each stringer-feet imperfection type. The sensitivity of the assembly strain results for different stringer-feet imperfection amplitudes is investigated next. In this section, the peak total hoop strains for three amplitudes for each stringer-feet imperfection type are compared to the peak strain values predicted for the flat-feet configuration.

For the heels-up condition shown in Fig. 10b, the peak strain values near each fastener for different stringer-feet imperfection amplitudes (20, 40, and 60 mils) are shown in Fig. 19. The peak total strains for this imperfection type are similar to those for the flat-feet configuration. Peak total hoop strain values occur near Fastener 4 as shown in Fig. 19. This response is due to the installation procedure of pushing the stringer down to the IT panel surface before installing the last eight fasteners. Because of the push-down installation procedure, the heels-up configuration becomes nearly the same as the flat-feet configuration as indicated in Fig. 19. Also note that irrespective of the amount of imperfection, the peak hoop strain in Fastener 4 is nearly the same.

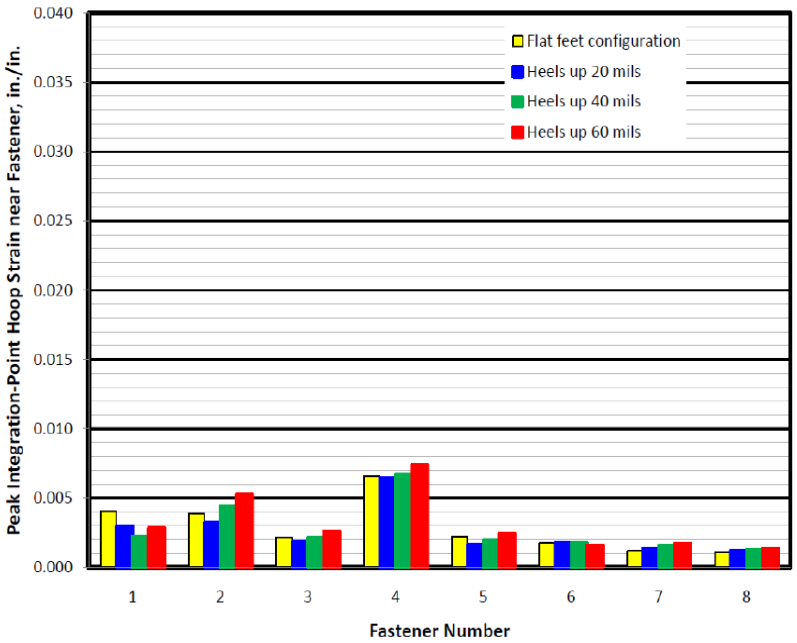

Figure 19. Peak hoop strain values near the first eight fasteners for the heels-up configuration for the assembly simulation.

For the diving-board condition shown in Fig. 10c, the total strain values near each fastener for different imperfection amplitudes (20, 40, and 70 mils) are shown in Fig. 20. These peak strain levels are similar to the strain levels for the flat-feet and heels-up configurations. Because of the installation procedure of pushing the stringer down prior to installation of the last eight fasteners, the peak assembly strains are not significantly different from those of the flat-feet configuration.

For the toes-up condition shown in Fig. 10d, the total strain values near each fastener for different imperfection amplitudes (20, 40, and 60 mils) are shown in Fig. 21. These strain levels are significantly different from those of the flat-feet configuration. For this imperfection type, the heels of the stringer feet cannot be pushed down to eliminate or minimize the distance the stringer toes are above the IT surface. Consequently, the stringer feet are brought into contact with the IT panel surface through the installation of the last eight fasteners. As a result, a significant increase in local strain levels occurs. As indicated in Fig. 22, the peak total hoop strains for the toes-up condition for increasing imperfection amplitude

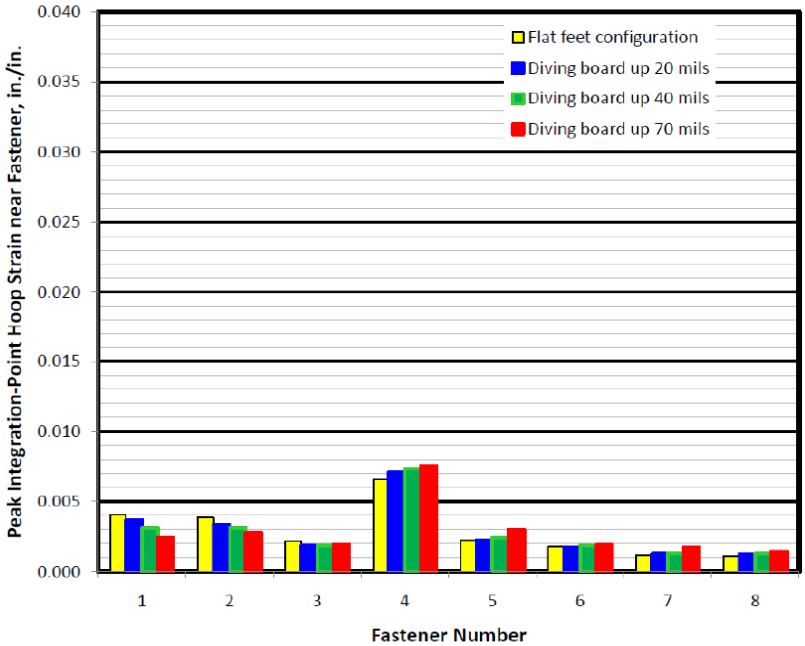

Figure 20. Peak hoop strain distributions near the first eight fasteners for the diving-board configuration for the assembly simulation.

follow a similar trend with a peak value occurring within the element group at Fastener 1 and reaching over 3 percent strain for the maximum imperfection amplitude of 60 mils. The peak values are tensile total hoop strains, and these peak values occur between the fastener and the stringer sidewall along the bottom of the stringer feet. The strain levels decrease to the level of the flat-feet configuration as Fastener 8 is approached where the stringer-feet imperfection vanishes.

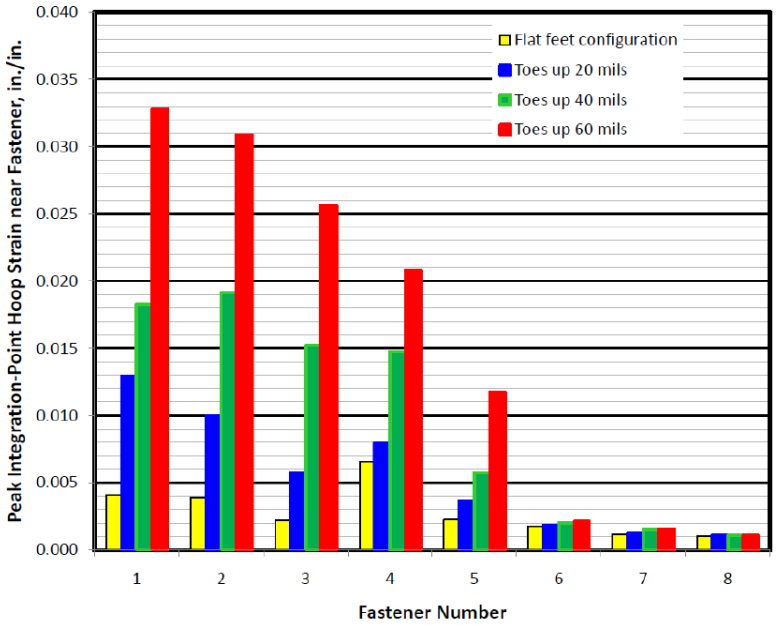

Figure 21. Peak hoop strain distributions near the first eight fasteners for the toes-up configuration for the assembly simulation.

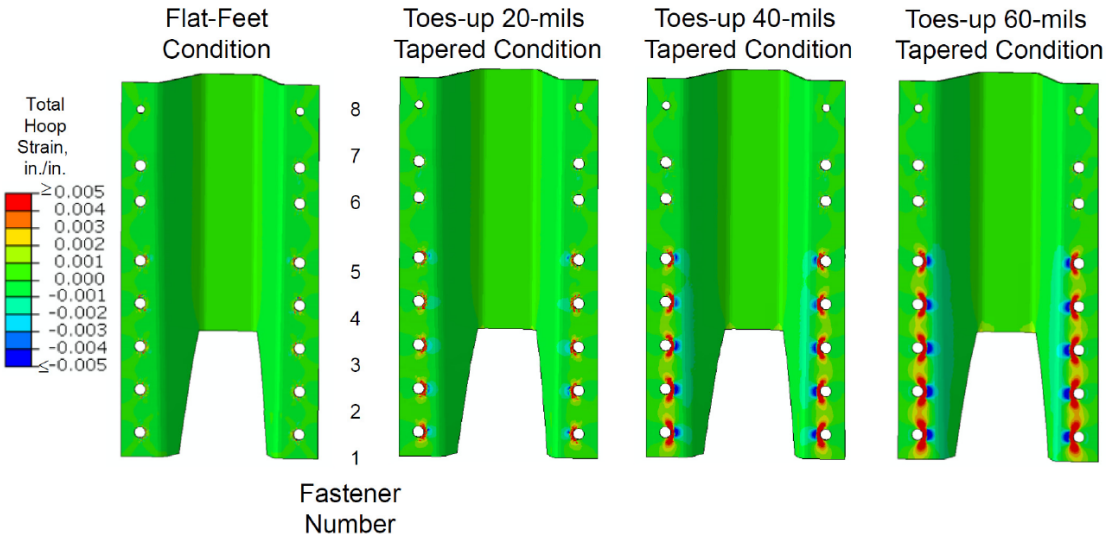

Figure 22. Total hoop strain distributions for the first eight fasteners after assembly for different amplitudes of the toes-up configuration – stringer-feet bottom surface.

D. Assembly Strains and Radius Blocks

The predicted assembly strains are influenced by many factors including stringer-feet imperfection type and amplitude, fastener preload, installation procedure, and part dimensions. In this paper, part dimensions, stringer-feet imperfection amplitude, installation procedure, and fastener preload are prescribed and not changed from case to case. Different stringer-feet imperfection types are examined for three steps of the installation process in Figs. 23 through 25. In subsequent bar-chart figures, the red bars denote the elastic part of the mechanical hoop strain, and the blue bars represent the plastic part of the mechanical hoop strain. In these figures, the red and blue bars are

stacked so that the individual height of a red or blue bar represents the hoop strain value for that part of the total strain. The tan bars in these figures represent the total hoop strain, which is the sum of the elastic and plastic hoop strain components.

The first step is after the installation of all fasteners and rivets. Recall that all rivets are installed at once in these simulations and then pairs of fasteners are installed sequentially. This step provides the initial conditions for the radius block installation procedure and for the operational loads assessment for the stringers *without* radius blocks as discussed in Ref. 4. The results shown in Fig. 23 are the peak hoop strains after the initial assembly of all fasteners for the four stringer-feet configurations. The initial assembly as simulated with the present models indicates plastic hoop strains for the first seven fasteners. Except for the toes-up configuration, the peak plastic hoop strains occur near Fastener 4 – just beyond where the stringer cap begins (see Fig. 15). Also, the highest assembly hoop strains develop for the toes-up configuration in the first two fasteners.

The second step is after Fasteners 2 through 7 have been removed in order to install the radius blocks. This step provides the initial conditions for the radius block installation procedure. The results shown in Fig. 24 indicate that plastic strains induced during the initial assembly (see Fig. 23) are locked in. Compressive elastic strains develop near all of the fasteners for all imperfections except near Fastener 1 for the heels-up and diving-board configurations. Recall that Fastener 1 remains installed for the radius block installation procedure.

The third step is after the installation of the radius blocks. This step provides the initial conditions for the operational loads assessment for the stringer *with* radius block cases discussed in Ref. 4. The results shown in Fig. 25 are similar to the previous peak hoop strain distributions near the first eight fasteners. The only noticeable difference is the increase in peak strains near Fastener 1 for the heels-up configuration after the radius blocks are installed.

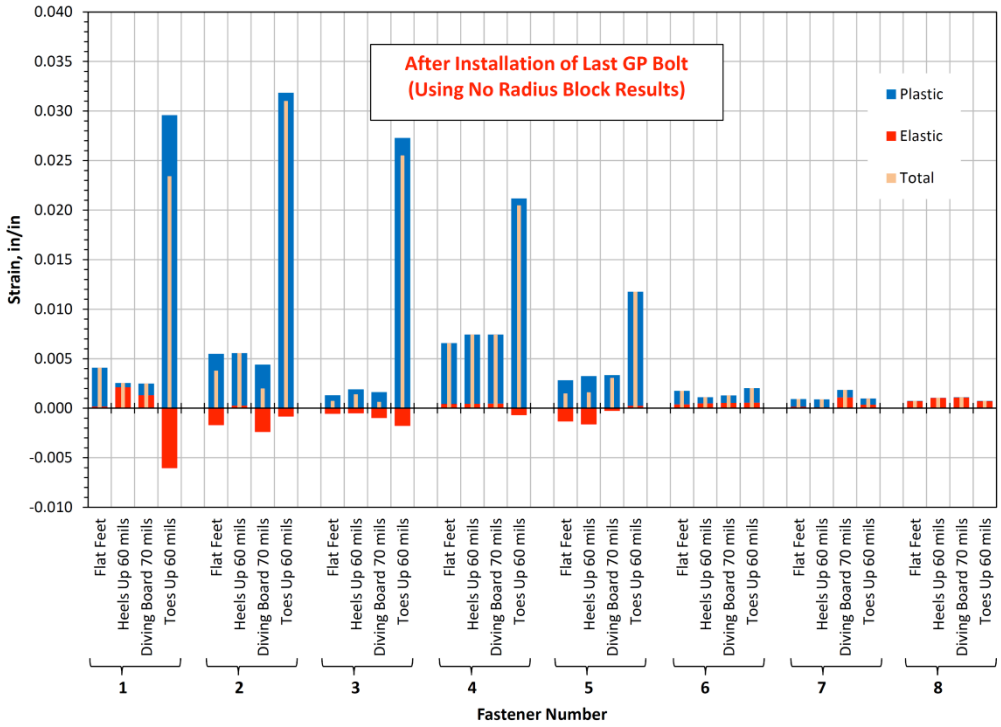

Figure 23. Peak hoop strains for the first eight fasteners after initial assembly of all fasteners for four stringer-feet configurations.

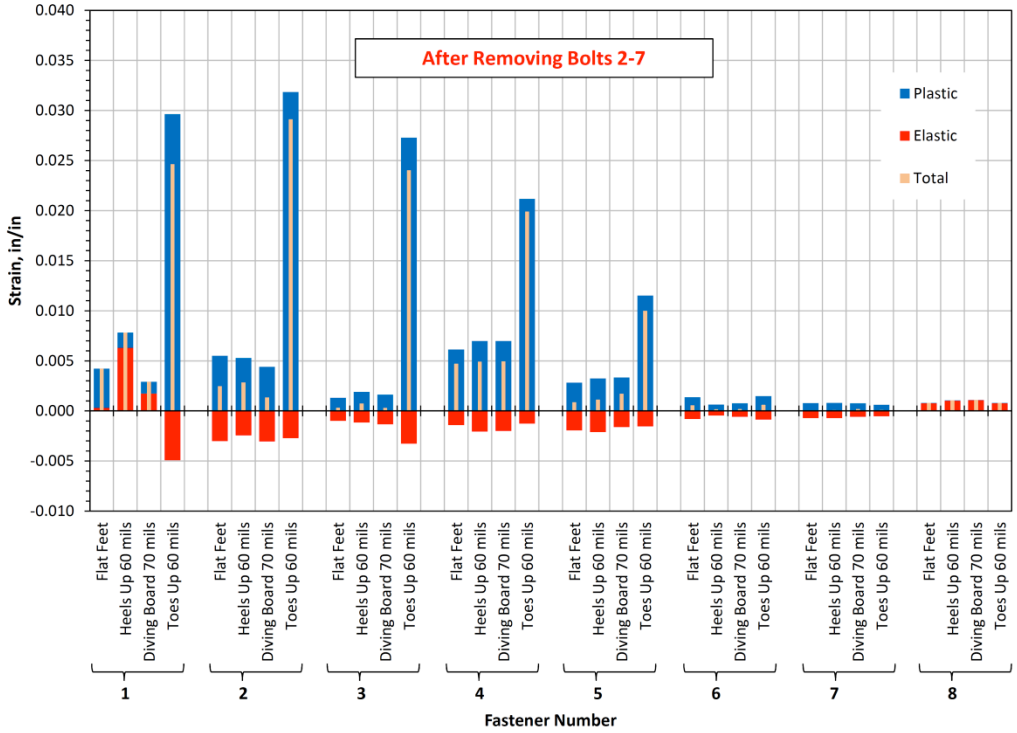

Figure 24. Peak hoop strains for the first eight fasteners after removal of Fasteners 2 through 7 and prior to radius block installation for four stringer-feet configurations.

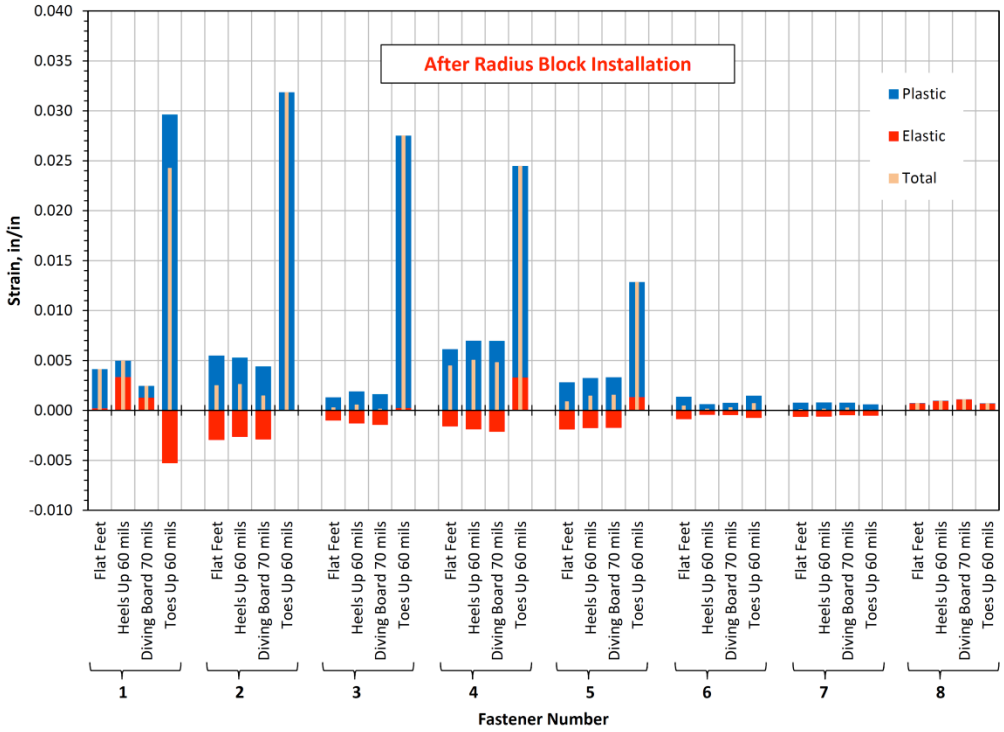

Figure 25. Peak hoop strains for the first eight fasteners after installing the radius blocks for four stringer-feet configurations.

V. Concluding Remarks

During the filling of the ET with cryogenic liquid fuels for the last mission of the Space Shuttle *Discovery*, cracking in the foam on an IT panel near the LOX tank interface was observed. Upon further inspection, it was discovered that not only was the foam cracked but also two external hat-shaped stringers under that foam on the IT had long cracks along the stringer feet between the fasteners and the stringer sidewall. Detailed 3D FE models were developed and analyzed to investigate the stringer elastic-plastic response and to assess the potential for local failure to develop in the stringer feet.

Elastic-plastic, large-deflection nonlinear stress analyses were performed for the external hat-shaped stringers (or stiffeners) on the IT portion of the Space Shuttle's ET. These stringers were subjected to assembly strains when the stringers are initially installed on an IT panel. Four different stringer-feet configurations including the baseline flat-feet, the heels-up, the diving-board, and the toes-up configurations were examined analytically using the stringer-push-down assembly procedure. The von Mises stress distributions after assembly indicated that localized plasticity will develop around the first eight fasteners. However, only the toes-up configuration resulted in high assembly hoop strains.

Assembly resulted in a multi-axis combined stress state that exceeds the material's uniaxial elastic yield limit for all IT stringer-feet imperfections considered, including the flat-feet configuration. The location, size, and amplitude of the strain field associated with the stringer assembly were sensitive to the assumed geometry and assembly procedure. These assembly simulations indicated that the assembly procedure as simulated in these analyses generate significant tensile strain levels in the bottom of the stringer feet. In particular, the toes-up configuration generated the highest strain levels.

The results of the assembly simulations from this paper were used in conjunction with operational mechanical and thermal loadings to assess IT stringer structural response and confirm that the radius blocks on the stringer-feet ends increased capability.

References

[1]Anon., *Space Shuttle External Tank System Definition Handbook, Volume II Layout Drawings*, LMC-ET-SE61-1, DR SE61 WBS 3.6.6, NAS8-26200, December 1997.

[2]Nemeth, M. P., Britt, V. O., Collins, T. J., and Starnes, J. H., Jr., "Nonlinear Analysis of the Space Shuttle Superlightweight External Fuel Tank," NASA TP-3616, December 1996.

[3]Gentz, S. J., "Space Transportation System (STS)-133/External Tank (ET)-137 Intertank (IT) Foam Crack and Repair Assessment," NESC-RP-10-00680, 2012. (Also available as NASA/TM-2012-217338, February 2012.)

[4]Knight, N. F., Jr., Song, K., Elliott, K. B., Warren, J. E., and Raju, I. S., "Space Transportation System (STS)-133/External Tank (ET)-137 Intertank (IT) Foam Crack and Repair Assessment: Elastic-Plastic Thermo-Mechanical Nonlinear Structural Analyses," NASA TP, 2012.

[5]Knight, N. F., Jr., Warren, J. E., Elliott, K. B., Song, K., and Raju, I. S., "Elastic-Plastic Nonlinear Response of a Space Shuttle External Tank Stringer: Part 2 – Thermal and Mechanical Loadings," Paper to be presented at the *53rd AIAA/ASME/ASCE/ATTS/ASC Structures, Structural Dynamics, and Materials (SDM) Conference*, Honolulu, Hawaii, April 23–26, 2012.

[6]Anon., *ABAQUS/Standard User's Manuals, Version 6.10*, Dassault Systèmes Simulia Corp., Providence, Rhode Island, 2010.

[7]Burkholder, J. T., "Calculation of Average Stress-Strain Curve for Al-Li 2090-T83 ET Stringer Material," MSFC M&P Laboratory, Flash Report No. MPFR-11-004, March 23, 2011.

[8]Anon., *Military Handbook: Metallic Materials and Elements for Aerospace Vehicle Structures*, MIL-HDBK-5H, Section 3.2.3, December 1, 1998.

[9]Knight, N. F., Jr., Phillips, D. R., and Raju, I. S. (2008). "Simulating the Structural Response of a Preloaded Bolted Joint," presented at the *AIAA/ASME/ASCE/AHS/ASC 49th Structures, Structural Dynamics, and Materials Conference*, Schaumburg, Illinois, April 7-10, 2008, AIAA Paper No. 2008-1842.

[10]Knight, N. F., Jr., Phillips, D. R., and Raju, I. S., "Ares I-X Upper Stage Simulator Structural Analyses Supporting the NESC Critical Initial Flaw Size Assessment," NASA TM-2008-215336, August 2008.

[11]Kim, J., Yoon, J.-C., and Kang, B.-S., "Finite Element Analysis and Modeling of Structure with Bolted Joints," *Applied Mathematical Modeling*, Vol. 31, 2007, pp. 895-911.

[12]Jerman, G. A., "ET-137 Stringer 7 Preliminary Fracture Analysis," MSFC presentation charts to CERB, November 23, 2010.

[13]Wells, D. N., "Key Questions, Answers, and Observations Concerning Al-Li 2090-T83 Stringer Material Behavior," MSFC M&P Laboratory, Flash report No. MPFR-11-013, February 2, 2011.

[14]Piascik, R. S., "Space Transportation System (STS)-133/External Tank (ET)-137 ET Foam Crack and Repair Assessment: Proximate Cause Determination and Material Characterization Study," NASA/TM-2011-217318, December 2011.